Lawrence Berkeley National Laboratory
Recent Work

Title
A Comprehensive Description of Transient Flow in Porous Media

Permalink
https://escholarship.org/uc/item/8f44m2ss

Authors
Kovscek, A.R.
Radke, C.J.

Publication Date
1993

eScholarship.org Powered by the California Digital Library
University of California

LBL-33604
UC-122

Lawrence Berkeley Laboratory
UNIVERSITY OF CALIFORNIA

EARTH SCIENCES DIVISION

Presented at the NIPER/DOE Symposium on Field Application of Foams for Oil Production, Bakersfield, CA, February 11–12, 1993, and to be published in the Proceedings

A Comprehensive Description of Transient Foam Flow in Porous Media

A.R. Kovscek and C.J. Radke

January 1993

LOAN COPY
Circulates
for 4 weeks
Bldg. 50 Library.
Copy 2
LBL-33604

Prepared for the U.S. Department of Energy under Contract Number DE-AC03-76SF00098

DISCLAIMER

This document was prepared as an account of work sponsored by the United States Government. Neither the United States Government nor any agency thereof, nor The Regents of the University of California, nor any of their employees, makes any warranty, express or implied, or assumes any legal liability or responsibility for the accuracy, completeness, or usefulness of any information, apparatus, product, or process disclosed, or represents that its use would not infringe privately owned rights. Reference herein to any specific commercial product, process, or service by its trade name, trademark, manufacturer, or otherwise, does not necessarily constitute or imply its endorsement, recommendation, or favoring by the United States Government or any agency thereof, or The Regents of the University of California. The views and opinions of authors expressed herein do not necessarily state or reflect those of the United States Government or any agency thereof or The Regents of the University of California and shall not be used for advertising or product endorsement purposes.

Lawrence Berkeley Laboratory is an equal opportunity employer.

This publication has been reproduced from the best available copy

DISCLAIMER

This document was prepared as an account of work sponsored by the United States Government. While this document is believed to contain correct information, neither the United States Government nor any agency thereof, nor the Regents of the University of California, nor any of their employees, makes any warranty, express or implied, or assumes any legal responsibility for the accuracy, completeness, or usefulness of any information, apparatus, product, or process disclosed, or represents that its use would not infringe privately owned rights. Reference herein to any specific commercial product, process, or service by its trade name, trademark, manufacturer, or otherwise, does not necessarily constitute or imply its endorsement, recommendation, or favoring by the United States Government or any agency thereof, or the Regents of the University of California. The views and opinions of authors expressed herein do not necessarily state or reflect those of the United States Government or any agency thereof or the Regents of the University of California.

LBL-33604

A Comprehensive description of Transient Foam Flow in Porous Media

A. R. Kovscek and C. J. Radke

Department of Chemical Engineering
University of California

and

Earth Sciences Division
Lawrence Berkeley Laboratory
University of California
Berkeley, California 94720

January 1993

This work was supported by the Assistant Secretary for Fossil Energy, Office of Oil, Gas and Shale Technologies, under U.S. Department of Energy Contract No. DE-AC03-76SF00098.

recycled paper

A Comprehensive Description of Transient Foam Flow in Porous Media

A. R. Kovscek and C. J. Radke*
Earth Sciences Division of Lawrence Berkeley Laboratory
and Department of Chemical Engineering
University of California, Berkeley
Berkeley, CA 94720

*Author to whom correspondance should be addressed.

Abstract

Efficient application of foam as a mobility-control agent for enhanced oil recovery requires a numerical model that can describe and predict its flow through porous media. Further, quantitative information on foam-flow behavior at reservoir flow rates and pressures is required for accurate field-scale modeling.

An experimental and mechanistic-modeling study is reported for the transient flow of foam through 1.3 μm^2 (1.3 D) Boise sandstone at backpressures in excess of 5 MPa (700 psi). Total superficial velocities range from as little as 0.42 to 2.20 m/day (1.4 ft/day to 7 ft/day). Sequential pressure taps and gamma-ray densitometry measure flow resistance and in situ liquid saturations, respectively. Thus, we generate experimental pressure and saturation profiles in both the transient and steady states.

A mechanistic foam simulator is created by incorporating a foam-bubble population balance[1] with the traditional reservoir simulation equations. Since foam mobility depends heavily upon its texture[2,3], the population balance is both useful and necessary as the role of foam texture must be incorporated into any model which seeks accurate prediction of flow properties. Our model utilizes saturation-dependent kinetic expressions for lamellae generation and coalescence and also a term for trapping of lamellae.

We find good quantitative agreement between experiment and theory in both the transient and steady states.

References and illustrations at end of paper.

Introduction

Foam is an excellent fluid for achieving mobility control of gases in porous media. Further, foam is relatively cost effective because it is mainly gas with stabilization of the gas/liquid interface provided by a relatively low concentration of surfactant (of order 1 wt%) within the aqueous phase. Since the gaseous portion of foam is dispersed, gas-phase flow mobility is greatly reduced and hence gravity override and viscous fingering through high-permeability streaks may be negated. However, practical implementation of foams for mobility control in enhanced oil recovery (EOR) processes has been hindered because a general understanding and a predictive model of foam flow does not exist.

Most previous studies were Eddisionian and focused upon the steady state. Although transient flow (i.e., displacement) is the most relevant to EOR, a reliable experimental data set that includes transient pressure and in-situ saturation profiles (along the length of a core) does not exist for foam flow. The most notable attempts at modeling foam flow have focused either on predicting transient flow[4] or on predicting steady state results[3,5], but not both. Additionally, the transient work of Friedmann et al[4] was for gas frontal advance rates between roughly 10 and 1000 m/day.

In recognition of the above issues, we undertook a simultaneous experimental and simulation study of transient foam displacement. We track experimentally the propagation of foam fronts within Boise sandstone at low displacement rates. Total superficial velocities in the transient mode are restricted to a maximum of 0.5 m/day (1.6 ft/day). Under steady state conditions, the liquid flow rate is varied while holding the gas flow rate constant (and vice versa) and measuring the resulting pressure drop behavior. Finally we model these results via a new population-balance simulator.

The purpose of this paper is to describe an easily implementable mechanistic simulator for foam displacement in porous media, to verify the theoretical results by comparison to experiment, and to identify areas of the model which may require further refinement. We concentrate on oil-free systems to avoid confusing foam propagation with foam/oil interaction. Before embarking on this task, it is helpful to describe how foam is configured within the pore space and to understand the pore-level events which alter the size and shape of foam bubbles.

Pore-Level Schematic of Foam Flow

Numerous pore-level phenomena control foam flow. The texture or number density of foam bubbles per unit volume strongly controls the actual flow resistance of foam. Individual foam bubbles encounter drag because of the presence of pore walls and pore constrictions, and because the gas/liquid interfacial area of a flowing foam bubble is constantly being rearranged by viscous and capillary forces[2]. Foam bubbles do not maintain their identity during transport. They are relentlessly destroyed and remade[26] according to the nature of the porous medium. Foam texture arises through a balance between varied and complicated foam generation and destruction mechanisms[6]. Additionally, all foam bubbles present in a porous medium are not flowing. Stationary foam severely reduces the permeability of a porous medium to gas by blocking many of the available flow paths. Dual-gas tracer studies[4,7] have measured the fraction of gas trapped within a foam at steady state to be between 85 and 99%.

Radke and Gillis[7] proposed Fig. 1 as a schematic for the pore-level distribution of foam. In this picture, cross-hatched circles are unconsolidated water-wet sand grains. Wetting fluid is denoted as the dotted phase. Foam bubbles are either unshaded or darkly shaded, depending upon whether they are trapped or flowing. The largest pore channels lie at the top of the figure while the smallest lie at the bottom. This orientation of pore channels is for ease of illustration.

Since there are strong capillary forces, wetting liquid occupies the smallest pore space and clings to the surface of sand grains as wetting films. The aqueous wetting phase maintains continuity throughout the pore structure shown in Fig. 1 so that aqueous-phase relative permeability is unchanged in the presence of foam[8]. Unshaded flowing foam transports as trains of bubbles through the largest and least resistive flow channels. If we adopt a continuum approach and speak of foam as a "phase," flowing foam becomes the least wetting phase in compliance with these strong capillary forces. Because the smallest pore space is occupied solely by aqueous phase and the largest pore space carries flowing foam, foam must trap (dark shading denotes trapped foam) in the intermediate-sized pores.

Foam reduces gas mobility in two manners. First, stationary or trapped foam blocks channels that otherwise carry gas. Second, bubble trains within the flowing fraction contain lamellae that interact with pore walls and thus a greater pressure drop is required to move gas through the porous medium than in the foam-free case. These trains are in a constant state of rearrangement. Bubbles transport a distance, are destroyed, and then reformed. Snap off is one mechanism by which foam is generated[9-11]. Intermittently, liquid fills a pore throat, is displaced by gas invasion, and subsequently a foam bubble is created if the pore throat to body aspect ratio is large enough (Fig. 2). It is also believed that bubble or lamellae division can play a role in generating fine bubbles[6,12]. Foam lamellae primarily break by a "stretching squeezing"[13] mechanism in oil-free porous media. When a lamella flowing from a pore throat into a body is stretched too rapidly it becomes unstable to infinitesimal disturbances and ruptures (Fig. 3). Because high capillary pressures thin lamellae by suction at Plateau borders, flowing lamellae are especially susceptible to rupture at low wetting saturations. More thorough reviews of foam generation, coalescence, and transport on the pore level are given in references 6 and 14.

We break the remainder of this paper into three sections. We begin by discussing our experimental apparatus, procedure, and experimental results. We then lay out a mechanistic but easily implemented one-dimensional population balance method that accounts for the propagation of foam and display both transient and steady state model results for a few test cases. Because foam in porous media displays flow properties very different from its individual constituent phases, it is mandatory that we use a method that incorporates the effect of foam texture on flow resistance. Next, we discuss the extent to which the theoretical predictions match experiment. Conclusions round out the paper.

Experiment

Apparatus

Persoff et al[15] originally constructed the apparatus (displayed schematically in Fig. 4) used for the experimental foam floods. The centerpiece of the apparatus is a vertically mounted, 60-cm long, 5.1-cm diameter, 1.3-μm^2 (1.3-D) Boise sandstone core with a porosity of 0.25. Thus, one pore volume corresponds to 300 cm^3. The core is epoxy-mounted into a 316 stainless steel sleeve designed to withstand pressures up to 20 MPa (3000 psi). A Mity-mite dome-loaded backpressure regulator (Grove Valve and Regulator Company, Emeryville, CA) maintains core backpressure.

Nitrogen gas and foamer solution are injected at the top of the core to prevent unwanted buoyancy driven gas flow. The original fluid injection system was replaced by a Brooks 5850C mass flow controller (Emerson Electric, Hatfield, PA) for nitrogen flow and an ISCO 500D syringe pump (Instrumentation Specialties Company, Lincoln, NE) for metering liquid flow. At 5 MPa (700 psi) backpressure, gas Darcy velocities between 0.30 and 2.1 m/day (1 to 7 ft/day) are now possible while liquid velocities as low as 0.009 m/day (0.03 ft/day) are employed.

Liquid saturation profiles are measured by scanning gamma-ray densitometry utilizing a 47 mCi Cs-137 source collimated to a 0.32 cm (1/8 in.) diameter beam. Gamma rays are detected by a Harshaw 5.1 cm (2 in.) NaI(Tl) scintillation counter and an NB-15X plug-on preamplifier (Harshaw Chemical Co., Solon, OH). Counting is performed by a Norland IT-5300 multichannel analyzer (Norland, Corp., Ft. Atkinson, WI) equipped with a digital gain stabilizer to compensate for drift. After a simple calibration where the intensity (counts/s falling within a 662 keV peak) of the gamma-ray beam is measured at preselected points along the core at 0% (I_d) and 100% liquid saturation (I_w), the liquid content at any previously calibrated point in the core is found from the Beer-Lambert law, $S_w = [\ln(I_d/I)]/[\ln(I_d - I_w)]$, where I is the intensity measured at any unknown saturation.

Scanning of the sandstone for liquid saturation profiles is achieved by mounting the gamma-ray source and detector on a translating carriage controlled by a Slow-syn motor (Superior Electric Company, Bristol, CT) and Model DPF107 motor controller (Anaheim Automation, Anaheim, CA). Since gamma rays are a product of radioactive decay, the square root of the number of events counted equals the standard deviation of the number of events counted. More accurate determinations of liquid saturation are found by using longer counting periods, however overly long counting periods reduce the precision of individual transient measurements and overall saturation profiles. The low frontal advance rates we use during transient foam displacements (a maximum of 0.5 cm/day) make it a relatively easy task to constrain the error in individual transient saturation measurements to about 4 saturation units with no loss in resolution of the advancing foam fronts. The error in steady state saturation measurements is less than 1 saturation unit.

Pressure taps are located at the core inlet, outlet, and at 10 cm (4 in.) intervals along the core, and are sealed with Swagelok O-seal (Crawford Fitting Company, Solon, Ohio) fittings. Pressure is measured using a single Paroscientific 43 KT piezoelectric quartz-crystal pressure transducer (Paroscientific, Redmond, WA). A Scannivalve 12L7 multiplexing valve (Scannivalve, San Diego, CA) allows all pressure taps to be visited sequentially and rapidly. A scan of all pressure taps is instantaneous (approximately 30 seconds) in comparison to the frontal advance rate. An HP-9000 (Hewlett Packard Co., Mountain View ,CA) controls the apparatus and records all data.

Procedure

The foamer solution is a saline solution containing 0.83 wt% NaCl (J. T. Baker, reagent grade) with 0.83 wt% active C_{14-16} α-olefin sulfonate surfactant (Bioterg AS-40, Stepan). Water is provided by a Barnstead Fi Streem II glass still (Barnstead, Thermolyne Corp., Dubuque, Iowa). The solution surface tension is 33 mN/m measured by the Wilhelmy plate method, and has a viscosity of 1 mPa·s. Bottled nitrogen is the gas source.

The core is first flushed with copious amounts (20-40 PV) of 0.83 wt% brine at 7 MPa backpressure. Periodically, the backpressure is released and then reapplied. This treatment removes virtually all gas from the core. Because trace amounts of isopropanol or methanol can have a deleterious effect on foam production, no alcohols are used as foam breakers or as cleaning solvents on any portion of the experimental apparatus. Following the surfactant-free preflush, at least another 5 PV of foamer solution is injected to satisfy rock adsorption of surfactant. Elemental analysis of the core effluent stream for sulfur reveals that after 2 PV of foamer solution is injected, the concentration of surfactant in the inlet and effluent streams is equal.

In all runs, liquid and gas are injected directly at a constant volumetric rate and a constant mass flow rate respectively. We do not foam the gas/liquid mixture before injection. The initial injection rates are not altered until a steady state pressure drop is achieved. The progress of foam propagation through the core is tracked by frequent pressure and saturation sweeps. After steady state is reached the liquid and gas rates are varied independently to reach a series of new steady states.

Results

We report first on the transient behavior when nitrogen and foamer solution are coinjected at constant rate. In the transient mode, we wish to determine the length of time required for the system to come to steady state and to verify the existence and track the movement of foam displacement fronts within the core. Then we examine the steady state behavior as gas or liquid solution flow rate is changed in a stepwise fashion. In the steady-state mode, our objective is to determine the effect of varying fluid flow rates on pressure drop (i.e., gas mobility) and to compare with previously published results[3,15].

Figures 5 and 6 give the transient saturation and pressure profiles, respectively. Experimental data points at each time level are connected by solid lines. Elapsed time is given nondimensionally in pore volumes (PV) which is the ratio of the total volumetric flow rate (at exit pressure) multiplied by elapsed time divided by the void volume of the core. Darcy velocities relative to the exit pressure are 0.43 m/day (1.4 ft/day) and 0.058 m/day (0.19 ft/day).

Steep saturation fronts are measured, whereby aqueous saturation upstream of the front is approximately 30%, about 5 units above connate, and downstream it is 100%. From the saturation profiles it appears that foam moves through the rock in a piston-like displacement. After the front passes a location, saturation changes very little. We find this rapid desaturation in all experiments. It is evident that a very efficient displacement of the aqueous phase is occurring. Even though nitrogen and surfactant solution are injected separately, rapid foam generation and liquid desaturation still occurs very near the core inlet. Gas breakthrough is at roughly 1.0 pv and little or no change occurs in the saturation profile after breakthrough. In general, we find that desaturation is complete 1 to 2 PV for all cases.

The pressure behavior of Fig. 6 confirms the existence of a strong foam piston moving through the core. Large pressure gradients are witnessed where aqueous phase saturation is low and vice versa. Further, Fig. 4 reveals that pressure profiles cease to change in roughly 3 PV also. The large pressure gradients with foam displayed in Fig. 4 are partly a result of the mode of fluid injection. If a surfactant alternating gas (SAG) process had been used, the measured gradients would be lower. Because foam is a dispersed gaseous phase separated by thin liquid films, forcing the two fluids to flow at a constant rate raises the pressure drop substantially.

The steady state results from varying the gas and liquid flow rates independently are shown in Figs. 7 and 8. For generality, we give pressure gradient information (i.e., the ratio of pressure drop to length) rather than core pressure drops. Figure 7 reports the pressure gradient behavior when gas injection velocity is held constant while varying liquid flow rate, whereas Fig. 8 shows the results from holding liquid injection rate constant but varying gas flow rates. In Fig. 7 the pressure gradient increases linearly from roughly 0.40 MPa/m to 3.6 MPa/m (18 to 160 psi/ft) as liquid velocity is varied between between 0.012 and 0.058 m/day (0.04 and 0.19 ft/day). For comparison, the pressure drop of water flowing at 0.46 m/day in 1.3 μm^2 (1.3 D) Boise sandstone is 4.2 kPa/m (0.18 psi/ft). Figure 8 illustrates that the pressure gradient remains fixed at approximately 1.4 MPa/m (63 psi/ft) while the gas velocity is varied between 0.43 and 1.90 m/day (1.4 and 6.2 ft/day). Again, the velocities reported are Darcy velocities relative to the exit pressure.

These steady state trends compare favorably with those previously published[3,15,16]. Namely, liquid saturations for steady state foam flow are a few units above connate and the pressure gradient is independent of gas velocity. We also reconfirm that steady state saturation for strong foam flow is a few units above connate (around 30% in this instance) and sensibly independent of both liquid and gas velocity. Persoff et al[15] also found that steady state pressure gradient increased linearly with liquid velocity.

A Foam Displacement Model

Our goal, in this section, is to outline a population-balance foam displacement model which is easy to implement, fits simply into the framework of current reservoir simulators, employs a minimum of parameters, but embodies pore-level events, and reproduces saturation and pressure drop versus flow rate results in both the transient and steady states. We begin first with the requisite material balance equations and then turn to incorporating foam into a typical reservoir simulation framework. We write equations for foam coalescence, generation, and lamellae flow resistance. Finally, we show selected one-dimensional numerical results and then compare results to the experimental data.

Conservation Equations

The mass balance equations for the gas and aqueous phases are written in standard reservoir simulator form[17,18]

$$\frac{\partial(\phi\rho_g S_g)}{\partial t} + \frac{\partial(\rho_g u_g)}{\partial x} = 0\,, \qquad (1)$$

and

$$\frac{\partial(\phi\rho_w S_w)}{\partial t} + \frac{\partial(\rho_w u_w)}{\partial x} = 0\,. \qquad (2)$$

In Eqns. (1) and (2), ϕ is the porosity of the porous medium, the subscripts g and w refer to the gaseous

and aqueous phases respectively, S_i is the saturation of each phase i, ρ_i is the density, and u_i the Darcy velocity of each phase.

The effective resistance of the gas phase is a strong function of foam texture[3,5]. Therefore, mechanistic prediction of foam flow in porous media is impossible without a conservation equation accounting for the evolution of foam texture[1]. Rates of accumulation, trapping, convection, generation, and coalescence of foam bubbles must be incorporated into a separate balance, analogous to inclusion of polymer into a reservoir simulator. Following Patzek[1], (c.f. also, 4 and 5) we write a transient one-dimensional population balance on the average flowing bubble size

$$\frac{\partial[\phi(S_f n_f + S_t n_t)]}{\partial t} + \frac{\partial(u_f n_f)}{\partial x} = \phi S_g(r_g - r_c), \qquad (3)$$

where the subscripts f and t refer to flowing and trapped foam respectively, n_f is the number of bubbles per unit volume of the flowing foam (i.e., the texture), and the total gas saturation is given by $S_g = S_f + S_t$. The first term of the time derivative is the rate of accumulation of flowing foam while the second is the rate of foam trapping. The spatial term tracks the convection of foam bubbles. On the right side of Eqn. (3), we express generation and coalescence rates, r_g and r_c, on per volume of gas basis. Hence, they are multiplied by porosity and gas-phase saturation. We turn next to constructing rate equations for the generation and coalescence of foam.

Coalescence Rate

A pore-level rate expression for foam coalescence is easy to write. Figure 3 illustrates that foam lamellae or bubbles are destroyed in proportion to their flux (i.e., $v_f n_f$) into termination sites[6]. Hence, we write

$$r_c = k_{-1}(S_w)\, v_f n_f, \qquad (4)$$

where $k_{-1}(S_w)$ is a coalescence rate constant which varies with local aqueous-phase saturation, S_w, and correspondingly capillary pressure. Additionally, v_f is the local interstitial velocity ($v_f = u_f/\phi S_f$). Eqn. (4) teaches that higher interstitial gas velocities lead to increased foam coalescence.

The saturation dependence of $k_{-1}(S_w)$ is quite dramatic. Khatib et al[19] have shown that for strongly foaming solutions $k_{-1}(S_w)$ is small for high aqueous phase saturations but rises steeply as S_w decreases. Since rapidly stretched lamellae become very thin, they are fragile and vulnerable to breakage. Sufficient time at low aqueous phase saturations does not exist for surfactant solution to flow into a rapidly stretched lamella thereby thickening and stabilizing it[13]. In fact, the study of single foam films has shown that a single limiting capillary pressure (P_c^*) exists for film breakage[20,21] depending strongly upon surfactant formulation and concentration. When P_c^* is met or exceeded foam films spontaneously rupture. Thus, an aqueous phase saturation near or below that corresponding to P_c^* leads to a rate of foam coalescence approaching infinity[19]. Cognizant of these facts we write

$$k_{-1}(S_w) = k_{-1}^{o}\frac{(1 - S_w)}{(S_w - S_w^*)}, \qquad (5)$$

where S_w^* is the saturation corresponding to P_c^*. Figure 9 displays schematically the coalescence rate versus saturation dependence.

Generation Rate

In writing a rate expression for generation by capillary snap-off we must point out that the necessary conditions are the accumulation of liquid at a pore throat and a disturbance in the gas liquid interface sufficient to cause breakup and rearrangement of the invading gas thread. Figure 2 illustrates the pore-level events leading to the formation of a foam lamella by snap-off. The rate of liquid accumulation is hence controlled by the local flow of foamer solution, v_w, into the pore throat, whereas the size of the bubble generated per snap-off event depends upon v_f. These conditions translate to dependence of foam generation by snap-off in both liquid and gas velocity. Thus, we simply write

$$r_g = k_1 v_f^a v_w^b, \qquad (6)$$

where a and b are power indices. The generation rate constant, k_1, reflects the number of foam germination sites. As long as the concentration of surfactant in the aqueous phase remains constant and the aqueous phase saturation remains above S_w^*, we assume that k_1 has little saturation dependence. Otherwise, when S_w falls below S_w^* sufficient liquid does not accumulate at pore throats for snap-off and the generation rate falls to zero.

Some researchers have found a velocity dependence for the onset of foam generation[4,9]. For foam generation at steady liquid saturation, Friedmann et al[4] report critical velocities of several hundred meters per day in some cases. They generate foam in a core where rock adsorption of surfactant is apparently satisfied, but the initial S_w is variable and low. Recent experiments in glass beadpacks, Boise,

and Berea sandstone, however, do not confirm the existence of a critical gas velocity or pressure drop which must be exceeded for successful foam generation[15,22-25] when the porous medium is presaturated with surfactant solution and foam generation occurs in a displacement process. We choose an initial S_w of 100 % and do not write a velocity criterion for the onset of generation.

Figure 9 displays the dependence of both coalescence and generation on S_w. Intersection of the two curves is set by the limiting capillary pressure, $P_c^*(S_w^*)$, which in turn sets the steady state saturation. The intersection is a stable point. If the system is perturbed away from this point, it naturally returns. Because we have explicitly written individual equations for foam generation and coalescence, this model reflects the relentless process of foam destruction and rebirth occurring within a porous medium[26]. To mimic the steady state flow rate pressure drop trends of Figs. 7 and 8, foam texture readjusts every time a change in either gas or liquid flow occurs.

As mentioned earlier, bubble division is another mechanism which creates flowing foam. The rate of bubble or lamellae division is proportional to the flux of lamellae into division sites. Thus, the rate of foam generation by division is similar in form to Eqn. (4). The difference between the coalescence rate and the generation rate by division is the value of the rate constant. However, both rate constants share the property of being small when S_w is high. More division sites become available as S_w drops increasing the likelihood of division. If significant bubble division does occur, an apparent lower coalescence rate is realized. It is difficult to separate division and coalescence. We do not attempt to do so here[3].

Effective Viscosity

Application of Eqns. (5) and (6) demands knowledge of the velocities of the gas and aqueous phases. Since foam behaves effectively as a nonwetting phase, Darcy's law,

$$u_f = \frac{K\, k_{rf}}{\mu_f}\left(\frac{-\partial p_g}{\partial x}\right), \qquad (7)$$

is employed here to describe foam flow behavior. In Eqn. (7), u_f, K, k_{rf}, μ_f, and p_g are the gas superficial velocity, absolute permeability, gas-phase relative permeability, foam effective viscosity, and gas-phase pressure, respectively. Water-phase Darcy velocity is similarly written. Darcy's law is not strictly obeyed in Eqn. (7) because foam is in general nonNewtonian.

The effective viscosity of flowing foam in porous media is generally an order of magnitude or two larger than gas viscosity alone. Experimentally, μ_f is calculated from Eqn. (7). Modeling of foam flow, though, requires a functional form. Two properties are generally included in all models of μ_f. First, the shear thinning or velocity dependence of foam is acknowledged. The notion that effective viscosity is a function of the foam texture, or number of lamellae per unit volume, is also included. Finer textured foams compel a larger flow resistance.

Friedmann et al[4] introduced an expression for effective viscosity that directly incorporates foam texture and velocity dependence. We adopt a slightly modified version

$$\mu_f = \mu_g + \frac{\alpha\, n_f}{v_f^c}, \qquad (8)$$

where α is a constant of proportionality. According to Eqn. (8) foam viscosity increases linearly with foam texture but decreases with increasing interstitial velocity. Friedmann et al[4] report an empirical value of 0.29 for the exponent c while the theoretical value is 1/3[2,27].

Trapped Foam

The fraction of foam trapped in a porous medium controls the fraction and rate of foam able to propagate and, along with effective foam viscosity, sets the pressure gradient. The fraction of foam that is trapped, $X_t = S_t/S_g$, is a currently unknown function of pressure gradient, capillary pressure, aqueous phase saturation, and pore geometry. Conversely, the flowing foam fraction is written $X_f = S_f/S_g$. Thus far, trapped gas fraction has only been successfully measured for experimental systems at steady state[4,7]. Percolation models, though, hold much promise for determining the functional dependence of X_f[28-33]. We write the trapped fraction as a function of n_f, which in turn is set by S_w and v_f,

$$X_f = 1 - (1 - X_{f,eq})\left(\frac{A_1 A_2 n_f}{1 + A_1 n_f}\right), \qquad (9)$$

where A_1 and A_2 are bubble trapping parameters and $X_{f,eq}$ is the flowing foam fraction at steady state exclusive of inlet or end effects. Equation (9) makes X_f equal to 1 when no flowing foam is present and allows X_f to decline smoothly to its equilibrium value as foam texture becomes finer. Both Eqns. (8) and (9) embody the experimental fact that finer textured foams lead to larger flow resistances. A reduced flowing foam fraction increases flow resistance by reducing gas-phase relative permeability.

Relative Permeabilities

For simplicity, a standard Corey exponent model is adopted for relative permeability functions. Water-phase relative permeability is unaffected by the presence of foam[8], hence

$$k_{rw} = k^{\circ}_{rw} \bar{S}_w^{g}, \tag{10a}$$

where

$$\bar{S}_{wd} = \frac{(S_w - S_{wc})}{(1 - S_{wc})}, \tag{10b}$$

and S_{WC} is the connate aqueous phase saturation. A major portion of the gas in a foam flood is present as trapped foam and blocks gas flow. Thus, gas-phase relative permeability must be modified. The saturation of gas actually flowing, S_f, is used to evaluate relative permeability rather than the entire gas-phase saturation

$$k_{rf} = k^{\circ}_{rg}\left[X_f(1 - \bar{S}_w)\right]^{h}. \tag{11}$$

Thus, gas-phase relative permeability is a function of foam texture and is much smaller than the case of a free gas propagating through a porous medium at the same wetting liquid saturation.

Assumptions and parameter fitting

It is assumed that surfactant is present in equal concentration throughout the aqueous phase and that rock adsorption has been satisfied. Also assumed is that the size of trapped and flowing foam bubbles are approximately the same. This is a good assumption under conditions of coinjection of surfactant solution and gas. Foam undergoes relentless generation and coalescence. The flowing portion is in constant contact with the trapped fraction. The trapped fraction is thus dynamic. That is, some portion of foam bubbles in the trapped fraction constantly mobilize, but they are replenished by a part of the flowing foam fraction trapping. As a result, trapped and flowing foam have about the same texture and the temporal derivative in Eqn. (3) reduces to $\partial[\phi\,(n_f\,S_g)]/\partial t$. The aqueous phase is taken as incompressible, and since the gas phase is nitrogen, the ideal gas law is assumed[3,4]. Gravitational and capillary effects are neglected.

The usual parameters required for modeling continuum two-phase flow are absolute rock permeability and porosity, exponents and endpoints for relative permeability, and phase viscosities. We fit Eqns. (10) and (11) to the relative permeabilities reported by Persoff et al[15]. Our implementation of the population balance requires specification of generation and coalescence rate constants, the saturation (S_w^*) corresponding to P_c^*, the exponents a and b for the generation rate expression, the proportionality constant and velocity exponent for effective viscosity, and the parameters for the flowing foam fraction relationship. Table 1 lists all constants and parameters used. Table 1 shows that 10 additional parameters are needed for the population balance, whereas undispersed flow already requires 9 parameters.

Parameter values for the population balance portion of the model are determined chiefly by steady state trends. Specifically, steady state saturation, pressure drop profiles, and flowing foam fraction must be matched. Fortunately, this drastically narrows our range of parameter choices. Thus, we first choose S_w^* slightly above connate, 0.26, and $X_{f,eq}$ equal to 0.1 in accordance with previous studies[4,7].

The flow rate exponent for effective viscosity, c in Eqn. (8), is set to 1/3. This is the theoretical gas-velocity dependence[2] applicable at low rates and close to the previously reported empirical value of 0.29[4]. Next, exponents are required for the liquid and gas rates for foam generation in Eqn. (6). When the rate of coalescence (Eqn.(4)) is subtracted from the rate of generation (Eqn. (6)), the result set to zero (i.e., $r_g - r_c = 0$), and Darcy's law (Eqn. (7)) including the effective viscosity function is substituted for phase velocities, the resulting expression reflects steady-state pressure gradients. This equation only applies when bubble generation and coalescence are in equilibrium. To obtain pressure drops independent of gas velocity while liquid velocity is held constant we choose a = 1/3. Likewise, for a linear dependence between liquid velocity and pressure drop at fixed gas velocity choose b = 1.

The ratio k_1/k_{-1} sets the equilibrium bubble density (defined by the equation $r_g - r_c = 0$). We find steady state textures[3] on the order of 10^5 cm^{-3}. Equation (8) combined with the equilibrium texture now sets the value of the steady state pressure drop and consequently α. Finally, the magnitudes of k_1, k_{-1}, A_1, and A_2 are adjusted to confine the region of net texture refinement to be close to the inlet face of the porous medium. Thus, A_1 and A_2 are chosen such that $X_t = (1 - X_f)$ is 75% of its equilibrium value when n_f is 50% of its equilibrium texture. Although there are 10 parameters needed for implementation of the population balance method, steady state trends directly set 6 of them. The only liberty allowed in parameter adjustment lies in specifying the values of k_1 and k_{-1} (but not the ratio of the two) and the trapping parameters A_1 and A_2.

The preceeding procedure illustrates that only one set of transient saturation and pressure profiles along

with the accompanying steady state trends need to be determined. This is easily accomplished within one experimental run.

Equations (1) through (11) are incorporated in a standard finite difference implicit pressure explicit saturation (IMPES) simulator with standard upstream weighting of the phase mobilities and solved. The three primitive unknowns are pressure, gas-phase saturation, and bubble density. All calculations are made on a DEC 5900. Further numerical details are available elsewhere[24].

Comparison of Theory and Experiment

Figures 5 and 6 contain the model results in addition to the experimental saturation and pressure profiles. Theoretical results are presented as dashed lines. The theoretical saturation profiles track the experimental results very well. Because the dispersing action of capillary pressure has not been included in the model formulation, model fronts remain steep and sharp. The model further predicts that S_w is high at the core inlet. Aqueous saturation is around 76% at x/L equal to zero, but drops rapidly to approximately 30% by x/L equal to 0.2. Since no foam is injected, n_f is essentially zero at the inlet, effective viscosity is equal to gas viscosity, and consequently S_w is high. Minssieux[35] detected such a region of high S_w near the inlet of a sandpack. A region of net foam generation exists near the inlet by implication. Foam texture increases rapidly, but the region where rates of generation and coalescence are out of balance is finite. Additionally, the fraction of foam trapped is zero at the inlet and grows to $1-X_{f,eq}$. Unfortunately due to equipment limitations, few experimental data are available in this region.

The region of net foam generation is also witnessed in the transient pressure profiles of Fig. 6. Both the experimental and model results (dashed lines) show that pressure gradients near the inlet are not steep indicating that flow resistance is small. Steep gradients are found downstream of the inlet region. Recall that large gas flow resistance arises from a viscous resistance contributed by flowing lamellae and also from resistance contributed by stationary foam through reduction in relative permeability. Although it is not possible to decouple these two effects[36], both are necessary if one wishes to model accurately foam flow. The adjustment of viscous resistance by foam texture is essential if the nonNewtonian behavior of foam is to be mimicked. Further, the viscous contribution alone is not sufficient to create the large overall pressure drops while still maintaining a region of net generation and smaller pressure gradients near the inlet. Hence, we infer experimentally that foam texture must be coarse near the inlet and the fraction of foam flowing there large.

These inferences are born out in Fig. 10 which reports model predicted foam texture as a function of dimensionless distance and time. We cannot compare directly to experiment because no experimental method currently exists to measure bubble density in situ. At all time levels, foam bubbles are coarsely textured near the inlet, but beyond the first fifth of the core, foam texture becomes nearly constant at each time level. Figure 10 also confirms that foam moves through the column in a piston-like fashion consistent with the experimental data in Figs. 5 and 6. Further consideration of these three figures shows that the saturation, pressure, and foam texture fronts track exactly both experimentally and theoretically. High pressure gradients and fine foam textures are seen where liquid saturation is low and vice versa.

We notice one more interesting feature of Fig. 10. At times of 0.62 and 0.80 PV the bubble density downstream of the inlet region exceeds the foam texture at steady state. This effect arises because the compressibility of the gas is included. A foam bubble created upstream finds itself out of equilibrium with the local pressure (that is, smaller or more dense than the local pressure demands) when it transports downstream. Hence, the steady-state texture is overshot somewhat as finely textured flowing foam fills the initially liquid filled regions near the foam front. Coalescence forces coarsen the bubbles over time back to the equilibrium density. At steady state the foam texture decreases away from the inlet region. Essentially, the bubbles expands and hence their number density decreases as they flow downstream into lower pressure areas. No overshoot in bubble texture is found in the calculations when the gas is made incompressible.

The overshoot in bubble density also causes an overshoot in the system pressure drop. Because the foam is finely textured, its flow resistance and hence pressure drop are large. At roughly 1 PV the core pressure drop exceeds the steady state pressure drop by approximately 15 per cent, then declines and undershoots the steady state slightly, and finally reaches the steady state value. Figure 11 illustrates this effect fully by contrasting the experimental system pressure drop as a function of throughput with the theoretical. We see that the experiment also overshoots steady state pressure drop. The experimental overshoot occurs about 1 PV later than predicted, though.

This discrepancy is likely a result of assuming that trapped and flowing foam are always in equilibrium. Equation (9) is constructed so that the correct steady state pressure profile is achieved. However, pressure gradient, gas velocity, and pore-geometry are also important for bubble trapping[28-31] during transient foam displacement.

In the steady state we find excellent agreement among experiment and theoretical prediction. Figures 7 and 8 report the model pressure gradient behavior as solid lines. In Fig. 7, the model pressure gradient increases linearly and overlies the experimental points except for the slight depression at roughly 0.028 m/day. The independence of pressure drop is illustrated in Fig. 8. Unfortunately, model prediction of pressure drop (1.6 MPa/cm) is slightly greater than the experimental result (1.4 MPa/cm). This discrepancy is understood by comparing the constant liquid velocity (0.028 m/day) used in Fig. 7 to the results in Fig. 8. The only experimental point which did not fall on the model predicted line lies at 0.028 m/day. The data taken during that portion of the experiment appear to have slightly depressed pressure drops.

The steady state pressure drop trends are a result of the adjustment of foam texture as flow rates change. When gas velocity is varied under constant liquid flow rate conditions, foam texture becomes coarser, viscosity decreases, and constant pressure drop is maintained. When liquid velocity is increased while gas rates are held constant, foam texture increases linearly with v_w and hence viscosity is adjusted so that Newtonian behavior is found. Flow resistance adjusts itself because foam texture must comply with a constant capillary pressure and low aqueous phase saturation.

Conclusions

We have developed a foam displacement model based on the population-balance method that is readily incorporated into current reservoir simulators. The proposed method is not computationally intensive and results are readily obtained using standard numerical methods. Because our formulation is mechanistic, it is general. Thus, extension to CO_2 or steam foams is straightforward. In general, we find good quantitative agreement between experiment and theory in both the transient and steady states.

Direct incorporation of the role of foam texture in our population-balance foam displacement model is the key to its success. Foam texture governs foam flow in porous media. A change in the flow velocity of either wetting liquid or gas must be accomodated by a change in texture and in turn a change in flow resistance.

Specifically, we draw the following conclusions for foam flow in 1.3 μm^2 (1.3 D) Boise sandstone at 5 MPa backpressure and for total superficial velocities between 0.40 and 2.1 m/day:

1. During transient experimental foam flooding of an initially surfactant filled and saturated core, resistance to gas flow builds rapidly in time. Steady state is generally achieved in 3 PV or less.

2. Our proposed population-balance model predicts the location of saturation and pressure fronts accurately. Steady state is predicted to be achieved in about 1.5 PV.

3. In the transient and steady state modes, fine foam textures are predicted to lead to large pressure gradients and low liquid saturations, whereas coarse textures lead to lesser gradients and higher liquid saturations.

4. We reconfirm experimentally that foam pressure gradients are independent of gas velocity, and also that foam pressure gradient increases linearly with liquid velocity. We predict these experimental results exactly with our population-balance model.

5. We find both experimentally and theoretically that a region of net foam generation exists very close to the inlet face of a linear core. Unfoamed surfactant solution and nitrogen are converted rapidly into a finely textured foam in this region.

Nomenclature

A_1,A_2	bubble trapping parameters in Eqn. 9
a,b,c	velocity exponents in foam generation and effective viscosity expressions
g	wetting phase relative permeability exponent
h	nonwetting phase relative permeability exponent
k	rate constant, units depend on rate expression
k_{ri}	relative permeability
I	intensity of gamma-ray beam (counts/sec)
K	permeability (m^2)
n_f	number density of flowing foam (# of bubbles/volume of flowing foam)
p	phase pressure (Pa)
PV	total pore volumes injected
P_c	capillary pressure, p_{nw}-p_w (Pa)
r	foam generation or coalescence rate (#of bubbles/(time)(volume of gas))
S_i	phase saturation
t	time (s)
u	Darcy velocity of phase i (m/s)
v_i	interstitial phase velocity (m/s)
x	spatial variable (m)
X_i	foam fraction

Greek Letters

α	proportionality constant for effective viscosity
ϕ	porosity
μ_i	viscosity

Subscripts

1	denotes generation rate constant
-1	denotes coalescence rate constant
c	coalescence
f	flowing foam
fl	normalized flowing foam saturation
f,eq	flowing foam at equilibrium between generation and coalescence rates
g	denotes gas phase on p and μ
g	generation
nw	nonwetting phase
t	trapped foam
w	wetting phase
wd	normalized wetting phase saturation

Superscripts

o	denotes reference value of rate constant
*	value corresponds to the critical capillary pressure

Acknowledgement

P. Persoff provided invaluable assistance in setting up the experiments presented in this paper. This work was supported by the U. S. Department of Energy under contract No. DC03-76SF00098 to the Lawrence Berkeley Laboratory of the University of California.

References

1. Patzek, T. W.: "Description of Foam Flow in Porous Media by the Population Balance Method," in Surfactant Based Mobility Control Progress in Miscible-Flood Enhanced Oil Recovery;" Smith, D. H. Ed., ACS Symposium Series No. 373, 326-341 (1988).

2. Hirasaki, G. J. and Lawson: "Mechanisms of Foam Flow in Porous Media: Apparent Viscosity in Smooth Capillaries;" SPEJ (April 1985) 176-190.

3. Ettinger, R. A.and Radke, C. J: "Influence of Foam Texture on Steady Foam Flow in Berea Sandstone," SPERE (February 1992) 83-90.

4. Friedmann, F, Chen, W. H., and Gauglitz, P. A.: "Experimental and Simulation Study of High-Temperature Foam Displacement in Porous Media;" SPERE (February 1991) 37-45.

5. Falls,A. H., Hirasaki, G. J., Patzek, T. W., Gauglitz, P. A., Miller, D. D., and Ratulowski, T.: "Development of a Mechanistic Foam Simulator: The Population Balance and Generation by Snap-Off;" SPERE (August 1988) 884-892.

6. Chambers, K. T. and Radke, C. J.: "Capillary Phenomena in Foam Flow Through Porous Media," in Interfacial Phenomena in Petroleum Recovery, Morrow, N. R. Ed., Marcel Dekker Inc., New York (1991) Ch. 6 191-255.

7. Gillis, J. V.and Radke, C. J.: "A Dual Gas Tracer Technique for Determining Trapped Gas Saturation During Steady Foam Flow in Porous Media," SPE 20519, presented at 65th Annual Technical Conference, New Orleans, LA, September, 1990.

8. Bernard, G. G., Holm, L. W., and Jacobs, W. L.: "Effect of Foam on Trapped Gas Saturation and on Permeability of Porous Media to Water," SPEJ (December 1965) 295-300.

9. Ransohoff, T. C. and Radke, C. J.: "Mechanisms of Foam Generation in Glass-Bead Packs;" SPERE (May 1988) 573-585.

10. Gauglitz, P. A., St. Laurent, C. M., and Radke, C. J.: "An Experimental Investigation of Gas-Bubble Breakup in Constricted Square Capillaries," JPT (September 1987) 1137-1146.

11. Ransohoff, T. C., Gauglitz, P.A., Radke, C. J.: "Snap-Off of Gas Bubbles in Smoothly Constricted Noncircular Capillaries," AIChE Journal (May 1987) 753-765.

12. Shirley, A. I.: "Foam Formation in Porous Media, A Microscopic Visual Study," in Surfactant Based Mobility Control Progress in Miscible-Flood Enhanced Oil Recovery;" Smith, D. H. Ed., ACS Symposium Series No. 373, 234-257 (1988).

13. Jiménez, A. I. and Radke, C. J.: "Dynamic Stability of Foam Lamellae Flowing Through a Periodically Constricted Pore," in Oil-Field Chemistry: Enhanced Recovery and Production Stimulation, Borchardt, J. K.and Yen, T. F. Eds., ACS Symposium Series No. 396, 460 - 479 (1989).

14. Kovscek, A. R. and Radke, C. J.: "Fundamentals of Foam Transport in Porous Media," in Foams in the Petroleum Industry, Schramm, L. L. Ed., ACS Advances in Chemistry Series, to appear 1993.

15. Persoff, P, Radke, C. J., Pruess, K., Benson, S. M., and Witherspoon, P. A.: "A Laboratory Investigation of Foam Flow in Sandstone at Elevated Pressure;" SPERE (August 1991) 365-371.

16. De Vries, A.S.and Wit, K: "Rheology of Gas/Water Foam in the Quality Range Relevant to Steam Foam," SPERE (May, 1990) 185-92.

17. Aziz, K. and Settari, A.: Petroleum Reservoir Simulation, Applied Science Publishers LTD London (1979) 125-199.

18. Hillestad, J. G. and Mattax, C. C.: "Selecting the Numerical Solution Method," in Reservoir Simulation; Mattax, C. C. and Dalton, R. L. Eds., SPE Monograph Series Vol. 13, Ch. 6 57-61 (1990).

19. Khatib, Z. I., Hirasaki, G. J., and Falls, A. H.: "Effects of Capillary Pressure on Coalescence and Phase Mobilities in Foams Flowing Through Porous Media," SPERE (August 1988) 919-926.

20. Khristov, K, Krugljakov, P., and Exerowa, D.: "Influence of the Pressure in the Plateau-Gibbs Borders on the Drainage and the Foam;" Colloid and Polymer Sci. (257 1979) 506-511.

21. Bergeron, V and Radke, C. J.: "Equilibrium Measurements of Oscillatory Disjoining Pressure," to appear Langmuir (1993).

22. Ettinger, R. A.: Foam Flow Resistance in Berea Sandstone M.S. Thesis, University of California, Berkeley (1989).

23. Chou, S. I.: "Conditions for Generating Foam in Porous Media," SPE 22628, presented at 66th Annual Technical Conference, Dallas, TX, October, 1991.

24. Kovscek, A. R. PhD thesis, University of California, Berkeley, in preparation (1993).

25. Fagan, M. E.: The Stability of Foam and Pseudoemulsion Films and Foam Flow Through Glass Beadpacks MS Thesis, University of California, Berkeley (1992).

26. Holm, L. W.: "The Mechanisms of Gas and Liquid Flow Through Porous Media in the Presence of Foam," SPEJ (December 1968) 359-369.

27. Falls, A. H., Muster, J. J., and Ratulowski, J.: "The Apparent Viscosity of Foams in Homogeneous Beadpacks," SPERE (May 1989) 155-164.

28. Rossen, W. R. "Theory of Mobilization Pressure Gradient of Flowing Foams in Porous Media: I. Incompressible Foam;" JCIS 1990, 136(1), 1-16.

29. Rossen, W. R. "Theory of Mobilization Pressure Gradient of Flowing Foams in Porous Media: II. Effect of Compressibility;" JCIS 1990, 136(1), 17-37.

30. Rossen, W. R. "Theory of Mobilization Pressure Gradient of Flowing Foams in Porous Media: III. Asymmetric Lamella Shapes;" JCIS 1990, 136(1), 38-53.

31. Rossen, W. R.; Gauglitz, P. A. "Percolation Theory and Mobilization of Foams in Porous Media," AIChE 1990, 36(8), 1176-1188.

32. Chou, S. I. "Percolation Theory of Foam in Porous Media;" SPE/DOE 20239, presented at SPE/DOE 7th Symposium on Enhanced Oil Recovery: Tulsa, OK, April, 1990.

33. de Gennes, P. G.: "Conjectures on Foam Mobilization," Revue De L'Institut Francais Du Pe'trol (47(2) 1992) 249-254.

34. Perry, R. H. and Green, D. W. Eds.: Perry's Chemical Engineers Handbook 6th Edition, McGraw Hill Book Company, New York (1984) Ch. 3 113.

35. Minssieux, L.: "Oil Displacement by Foams in Relation to Their Physical Properties in Porous Media," JPT (January 1974) 100-108.

36. Rossen, W. R.: "Modeling Foam Mobility in Porous Media," SPE 22627, presented at 66th Annual Technical Conference, Dallas, TX, October, 1991.

Table 1: Parameter Values

Reservoir Simulation Parameters		Population Balance Method	
parameter	value	parameter	value
K	1.3 μm^2	k_1	5.13 E+5 $s^{1/3} cm^{-13/3}$
ø	0.25	k_{-1}^o	1.50 E-3 cm^{-1}
g	3.0	S_w^*	0.26
k_{rw}^o	0.70	a	1/3
h	3.0	b	1.0
k_{rg}^o	1.0	α	1.80 E-6 mPa s $s^{1/3} cm^{8/3}$
Swc	0.25	c	1/3
μ_w	1.0 mPa·s	$X_{f,eq}$	0.10
μ_g	0.018 mPa·s	A_1 , A_2	4.0, 1.25

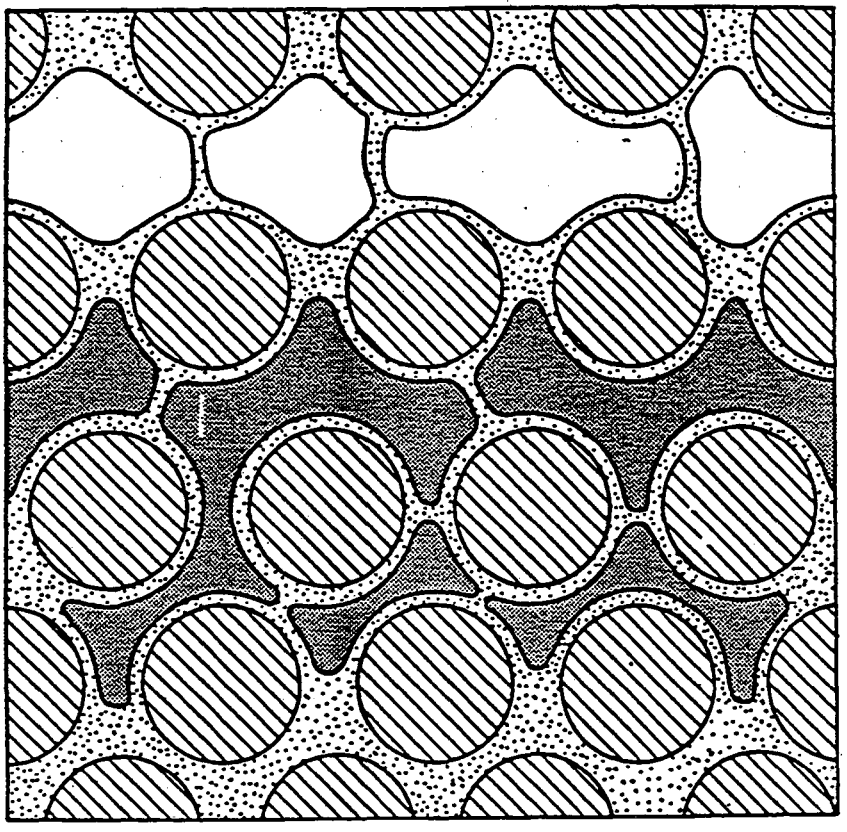

XBL 909-2973

Figure 1: Pore-level schematic for a flowing foam. Flowing bubbles are unshaded and trapped gas is darkly shaded.

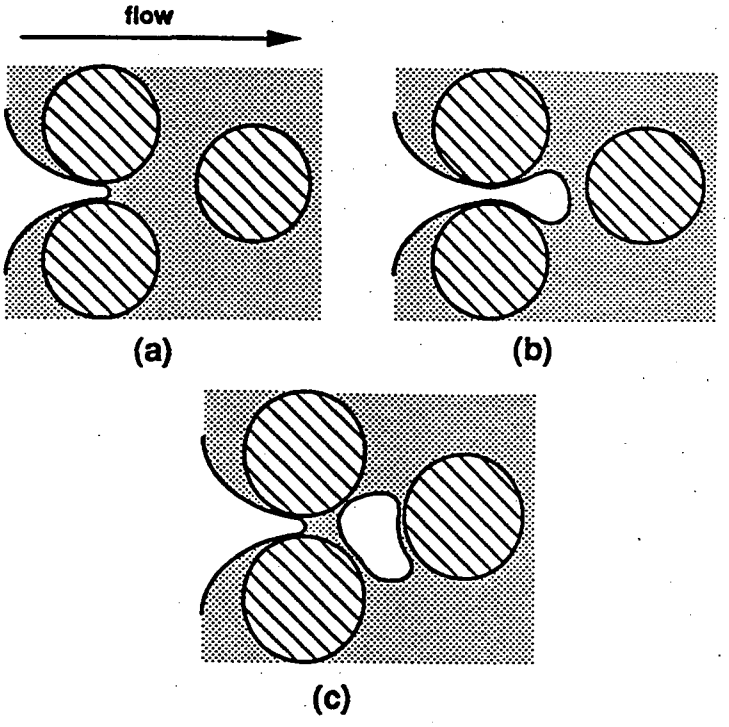

Figure 2: Schematic of snap-off mechanism. Gas is unshaded.

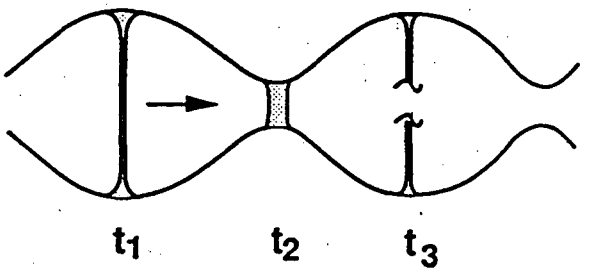

Figure 3: Foam lamella translating from left to right in a periodically constricted pore. Coalescence occurs at t_3 .

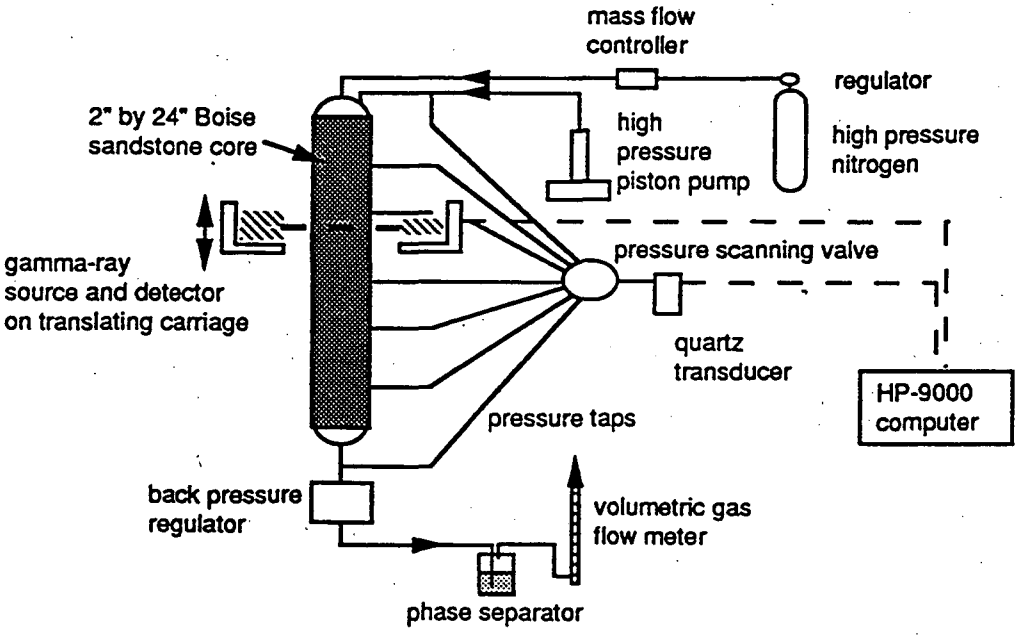

Figure 4: Apparatus for foam displacement experiments.

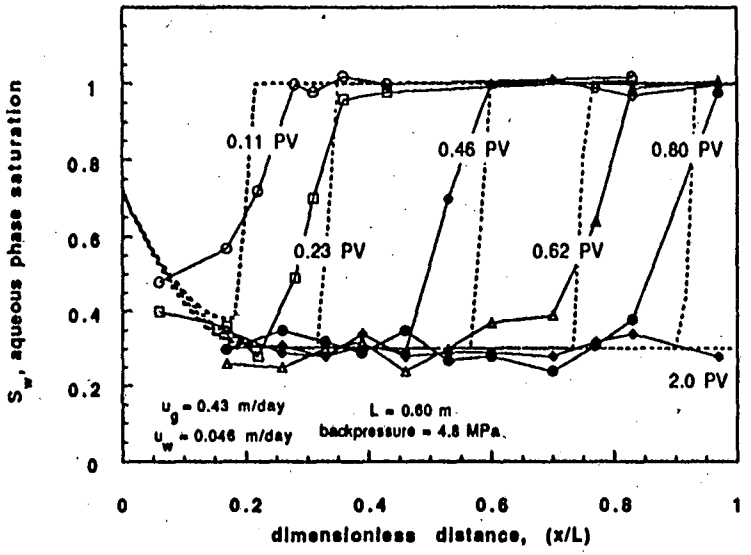

Figure 5: Experimental and model transient aqueous phase saturation profiles. Model results shown with dashed lines

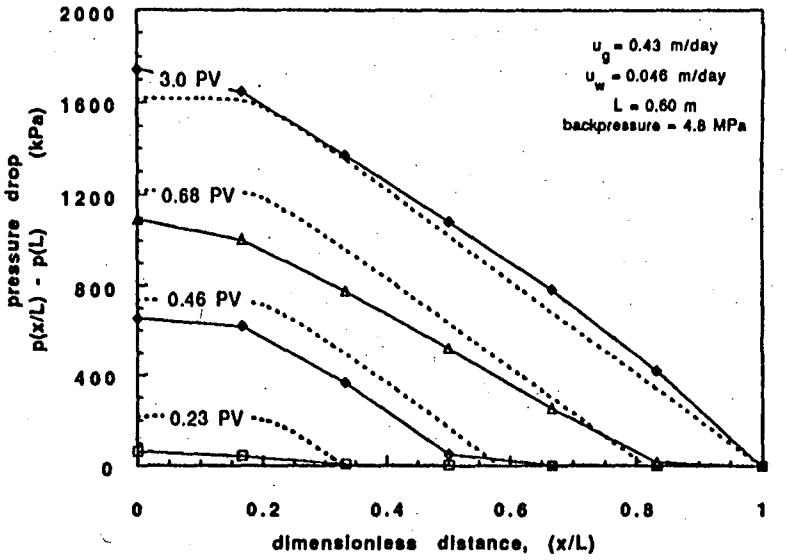

Figure 6: Experimental and model transient pressure profiles Model results shown with dashed lines.

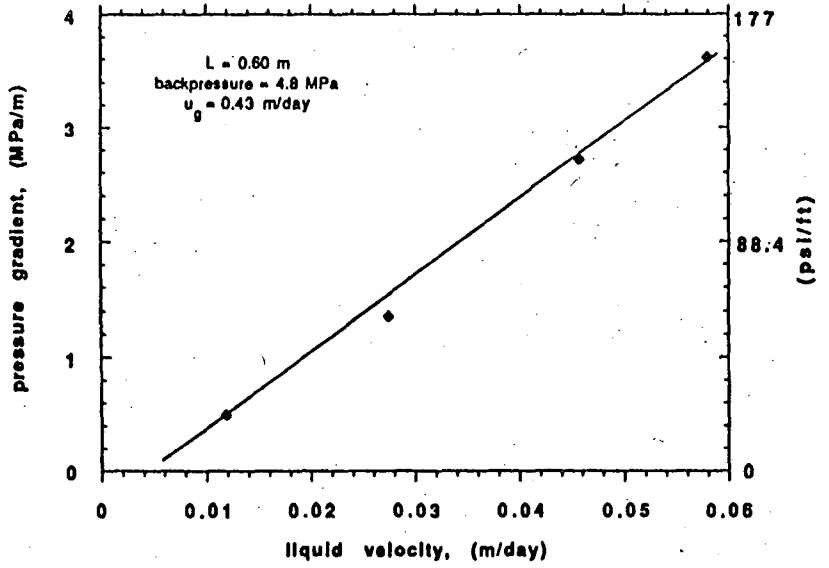

Figure 7 Experimental and model (solid line) steady state pressure gradient versus liquid velocity

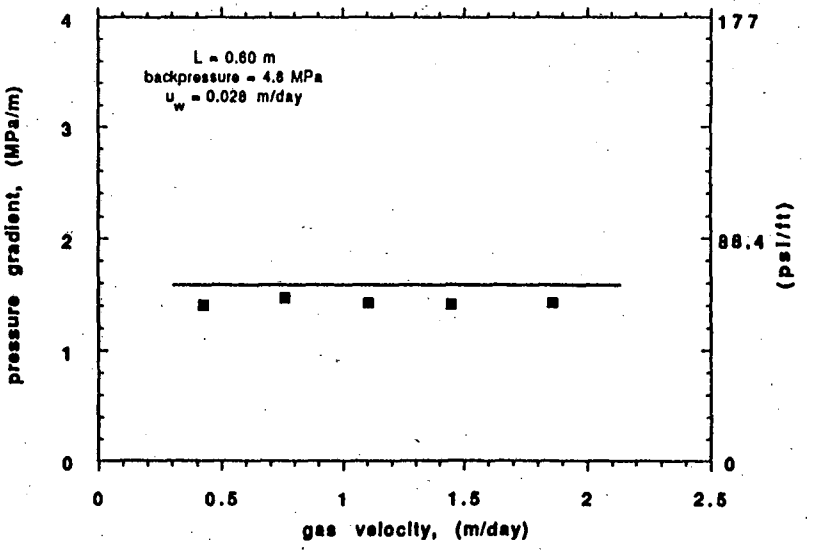

Figure 8: Experimental and model (solid line) steady state pressure gradient versus gas-phase velocity.

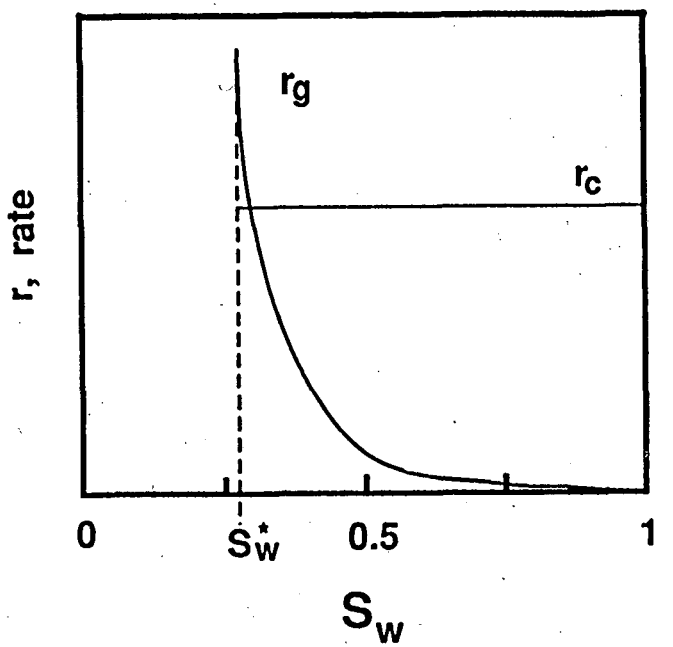

Figure 9: Generation and coalescence rates as a function of aqueous-phase saturation (schematic).

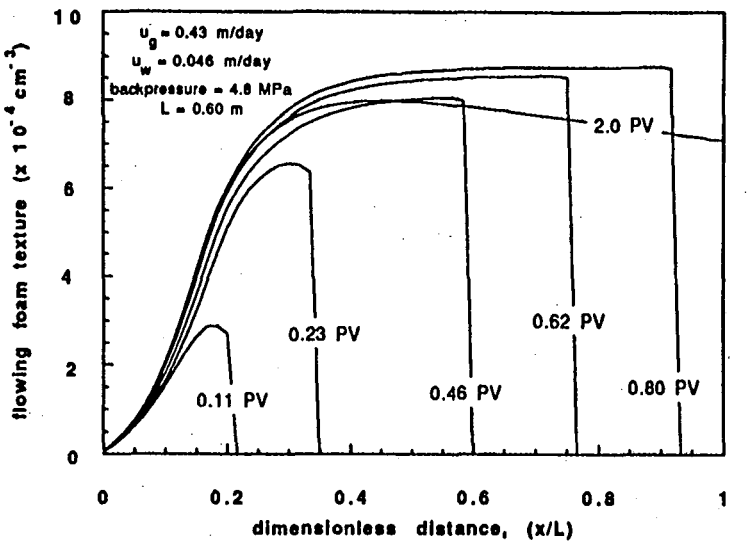

Figure 10: Model transient flowing foam textures.

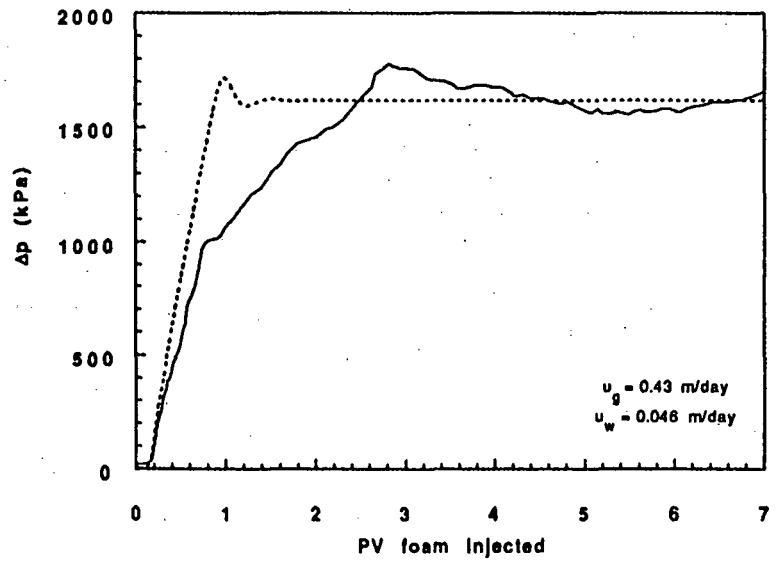

Figure 11: Experimental and model core pressure-drop history. Model results shown with dashed lines.

LAWRENCE BERKELEY LABORATORY
UNIVERSITY OF CALIFORNIA
TECHNICAL INFORMATION DEPARTMENT
BERKELEY, CALIFORNIA 94720

ABH589
LBL Libraries